Spectrum Width Measured by WSR-88D: Error Sources and Statistics of Various Weather Phenomena

MING FANG

Cooperative Institute for Mesoscale Meteorological Studies, University of Oklahoma, Norman, Oklahoma

RICHARD J. DOVIAK

National Severe Storms Laboratory, Norman, Oklahoma

VALERY MELNIKOV

Cooperative Institute for Mesoscale Meteorological Studies, University of Oklahoma, Norman, Oklahoma

(Manuscript received 16 June 2003, in final form 1 December 2003)

ABSTRACT

Spectrum widths, one of the three moments measured and displayed by the Weather Surveillance Radar-1988 Doppler (WSR-88D), are categorized for various weather conditions showing both expected and unexpected results. Weather phenomena are classified into seven categories based on radar observations, and the statistics of the censored spectrum width fields for each of the categories are obtained. Daytime fair weather without birds, stratiform rain and snow, and isolated tornadic storms produce weather signals that have the smallest volumetric median values of spectrum widths (i.e., < 2 m s^{-1}). Surprisingly, the median spectrum width values in the isolated tornadic storms are as low (i.e., <2 m s^{-1}) as in the fair weather (without the presence of echoes from birds). The median spectrum width value from fair weather regions contaminated with bird echoes is larger (i.e., 3.0 m s^{-1}). The largest median spectrum width values, ranging from 4.0 to 5.4 m s^{-1}, are associated with embedded areal squall lines. Clusters of severe storms and storms along broken squall lines appear to have median spectrum width values between these two regimes. Spectrum width fields are also shown to be more prone to errors than fields of reflectivity and velocity. Errors mainly result from overlaid echoes, improper automatic gain control (AGC) settings, low signal-to-noise ratios, and incorrect estimates of noise power. Thus spectrum width data fields require extensive censoring. The most persistent errors appear to be those related to overlaid weather signals and low signal-to-noise ratios.

1. Introduction

Spectrum width, σ_v, has the potential to improve the interpretation of weather radar data, which can lead to better warnings of severe weather (Lemon 1999; Bohne et al. 1997) and hazards to safe flight (Doviak 1999). Storm turbulence, a hazard to safe flight, is a main contributor to spectrum width (Istok and Doviak 1986), and spectrum width remains the principal means to detect regions dangerous for safe flight (Cornman et al. 1999). Nevertheless, the use of spectrum width data has been limited compared to reflectivity and Doppler velocity fields. This is due in part to the difficulty in relating σ_v to meteorologically significant phenomena (e.g., turbulence hazards to safe flight), and in part to the fact that σ_v values are easily corrupted (e.g., by overlaid echoes), and thus spectrum widths are less reliable and more risky to interpret.

Another motivation for this study is the capability of Doppler weather radar to resolve range and velocity ambiguities depends strongly on σ_v. Weather Surveillance Radar-1988 Doppler (WSR-88D) specifications (NOAA 1991) are based on analysis of limited data from research radars that showed median values of σ_v in three tornadic storms to be about 4 m s^{-1} (Doviak and Zrnić 1993). But tornadic storms comprise a small percentage of the weather being observed with Doppler radars. Theoretical studies on methods to mitigate the effects of ambiguities typically assume median $\sigma_v \approx 4$ m s^{-1}. Sachidananda et al. (1998) developed a family of systematic phase codes (i.e., the SZ codes), which, when used to modulate the phase of the transmitted signal, allows separation of overlaid weather signals. But the performance of these codes strongly depends on the widths of the overlaid Doppler spectra; if spectrum widths exceed about 1/5 of v_a (the Nyquist velocity),

Corresponding author address: Ming Fang, CIMMS, University of Oklahoma, 100E Boyd, Rm.1110, Norman, OK 73019-1011.
E-mail: ming.fang@noaa.gov

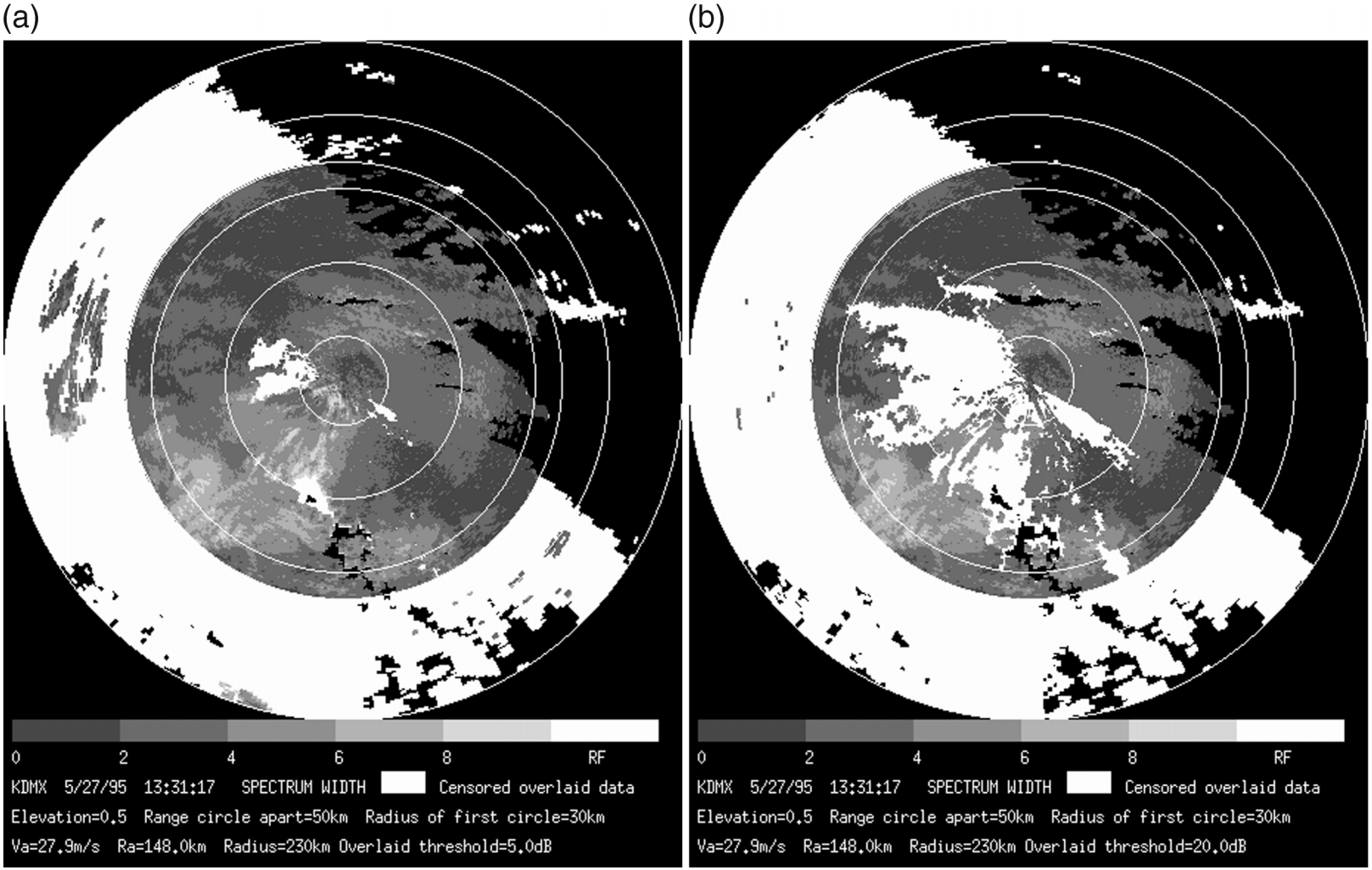

FIG. 1. (a) The spectrum width field censored with a 5-dB overlaid threshold. (The grayscale bar designates width values in m s^{-1}.) Data recorded by the WSR-88D in Des Moines IA, on 27 May 1995. The radius of first range-marking circle is at 30 km and the others are 50 km apart. The circle at 148 km is at the ambiguous range r_a. (b) Same as (a) but overlaid data were censored using a 20-dB overlaid threshold.

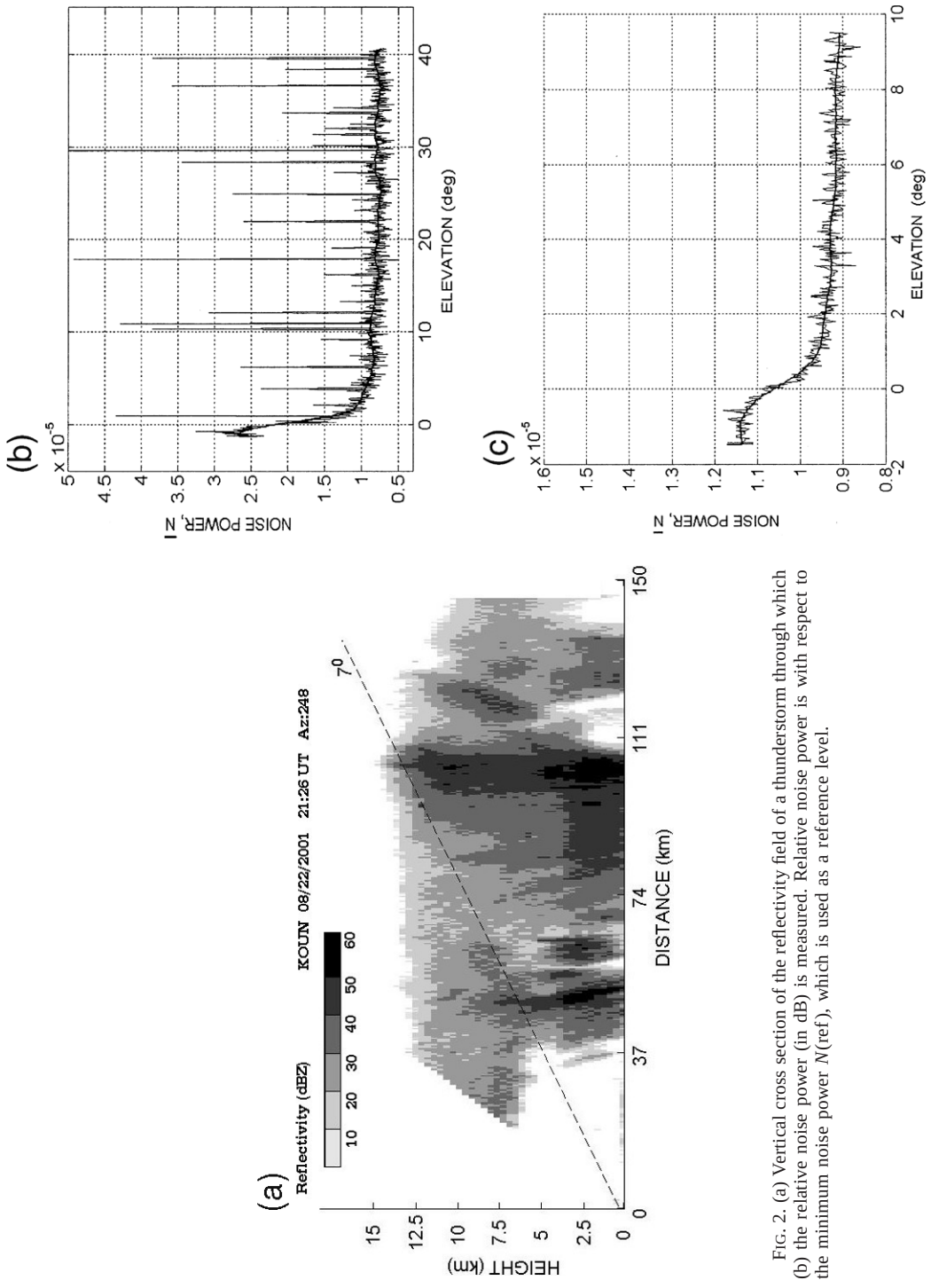

FIG. 2. (a) Vertical cross section of the reflectivity field of a thunderstorm through which (b) the relative noise power (in dB) is measured. Relative noise power is with respect to the minimum noise power $N(\text{ref})$, which is used as a reference level.

the performance of the algorithm rapidly deteriorates. Sachidananda et al. (1998) show that there is a significant increase in the variance of velocity and spectrum width estimates when σ_v exceeds about 5 m s^{-1} for pulse repetition times (PRTs) typically used by the WSR-88D (i.e., $21 < v_a < 32$ m s^{-1}). Although coding transmitted pulses can improve the performance of radar, the level of improvement depends on σ_v and, in turn, these depend on the type of weather being observed.

WSR-88D level II data are used herein to analyze spectrum width data because its widespread availability provides us with many opportunities to obtain a wide variety of weather for the study, and because the WSR-88D data are amenable to editing of erroneous data.

2. Error sources

It is well known that estimates of σ_v, the square root of second central moment of the Doppler spectra, are more prone to errors than the zeroth (power, or reflectivity) or the first (i.e., mean Doppler velocity) moment. So before performing any analysis and classification with the spectrum width data, erroneous data must be censored so that the resulting fields are relatively free from errors.

a. Errors due to overlaid echoes

If a scatterer's range is larger than the unambiguous range r_a ($r_a = cT_s/2$, where c is the speed of light, and T_s is the PRT), the reflected signal is received after the next pulse is transmitted, and then overlaid echoes can occur. Reflectivity observations with the WSR-88D always use sufficiently long PRTs so that there are no reflectivity errors due to overlaid echoes. On the other hand, Doppler velocity v and σ_v must be estimated using relatively short PRTs that often lead to conditions of overlaid weather signals corrupting the v and σ_v measurements.

If the in-trip echo power is more than $T_o = 20$ dB stronger than the sum of out-of-trip echo powers (T_o is the overlaid threshold), it can be shown that the spectral moments of the stronger signal can be estimated without significant error. That is, the NEXRAD technical requirements (NOAA 1991) are met. The overlaid threshold test in the WSR-88D compares the in-trip echo power (either in two azimuth surveillance scans at the same elevation angle but separated by about 20 s, or on two data radials separated by about 0.5°), obtained using long PRTs in each 1-km range-averaging interval $\Delta r = 1$ km (Doviak and Zrnić 1993), with the signal power in *each* of the out-of-trip Δr that would overlay the in-trip echoes. That is, the summed out-of-trip echo power is not used. In this study the overlaid threshold T_o is that level or larger above the *sum* of the out-of-trip echo powers that the in-trip echo power must achieve in order to declare that the estimates are valid. Comparing the in-trip echo power with the sum of out-of-trip powers is a more demanding criterion than comparing the powers individually from each out-of-trip region.

An example of spectrum width estimates being corrupted by overlaid echoes is shown in Fig. 1. Figure 1a shows a spectrum width field from stratiform rain with embedded weak convective elements observed with the WSR-88D in Des Moines, Iowa, on 27 May 1995. All reflectivity data are estimated during surveillance scans using long PRTs, which practically preclude overlaid echoes in the reflectivity field. But velocity and spectrum width are not estimated during these surveillance scans. Velocity and spectrum widths are calculated during separate scans about 20 s later at the same elevation angle using short PRTs for the 0.5° and 1.5° elevation cuts. But this results in shorter r_a and a large occurrence of overlaid echoes. The range circle at 148 km is at the r_a when Doppler velocity and spectrum width data are collected. The data presented in Fig. 1a were censored using an overlaid threshold $T_o = 5$ dB (typical of that used in the WSR-88D network since 1996). The areas defined by the range-folded (RF) gray level in Fig. 1a represent the areas of censored data for which the overlaid threshold is not exceeded. Many cell-like regions of large spectrum widths, at ranges between 30 and 83 km to the southwest, appear to be anomalous. Because the $T_o = 5$ dB overlaid threshold has censored some of the cores (e.g., the core at about 80 km and at an azimuth of about 195°) of these cell-like σ_v regions, it is concluded that second trip reflectivity fields, with echo powers stronger than the first trip ones by at least -5 dB, are overlaying the first trip data fields.

The high σ_v cells, and the regions of high σ_v values surrounding the censored data, are also likely corrupted. Using the larger overlaid threshold $T_o = 20$ dB (Fig. 1b), these areas of suspiciously high σ_v are censored. Furthermore, some areas of large spectrum widths ($\sigma_v = 3$ to 4 m s^{-1}) to the west-southwest between 80 and 110 km are censored using this higher T_o. These regions also have spectrum width estimates that are likely biased high by overlaid echoes.

But not all regions of overlaid echoes necessarily have corrupted σ_v values, even if they met the criterion for censoring. For example, if Doppler spectra of two overlaid weather signals have the same mean velocity and spectrum widths, the estimated width will be correct for both regions. Although censoring data based on power ratios cause the loss of some valid data, the resulting data fields are guaranteed to be free from errors due to overlaid echoes. Thus we allow the sacrifice of some valid spectrum width data to ensure that the analyzed data are free from errors due to overlaid echoes.

b. Errors due to incorrect estimates of noise power

Besides spectrum width estimates being corrupted by overlaid echoes, the spectrum width estimates are more prone to errors due to receiver noise, and to incorrect estimates $\overline{N}$ of true receiver noise power N, than are

velocity estimates (an overline on N is used to differentiate this estimate, which uses many more samples: 24 samples per range bin times 300 range bins = 7200, than the number of samples used to estimate spectral moments). By assuming a Gaussian-shaped power spectrum, the WSR-88D hardware calculates the autocovariance at lag 0 and 1 to estimate spectrum width, using the pulse-pair logarithm (PPL) formula [Doviak and Zrnić 1993; their Eq. (6.27)]:

$$\hat{\sigma}_v = \frac{\sqrt{2}v_a}{\pi}\left|\ln\left[\frac{\hat{S}}{|\hat{R}(T_s)|}\right]\right|^{1/2} \operatorname{sgn}\left[\ln\left(\frac{\hat{S}}{|\hat{R}(T_s)|}\right)\right], \quad (1)$$

where $\hat{R}(T_s)$ is the autocovariance function at lag T_s (i.e., at lag 1), and $\hat{S}$ is the estimate of signal power computed from $\hat{R}(0)$ and $\overline{N}$,

$$\hat{R}(1) = \frac{1}{M}\sum_{k=0}^{M-1} V^*(k)V(k+1); \qquad \hat{S} = \hat{R}(0) - \overline{N}, \quad (2)$$

$V(k)$ and $V(k+1)$ are the kth and $(k+1)$th samples of signal plus noise, $V^*(k)$ is the conjugate of $V(k)$, M is the number of samples (i.e., ≈50) used in estimating S and $R(T)$, and $\overline{N}$ is the noise power measured during the calibration of the radar. As explained later in this section, the sgn function is used to flag spectrum widths for which the argument of the logarithmic function is less than unity; this gives imaginary values for spectrum widths.

Noise calibration takes place during the elevation angle θ_e retrace period at $\theta_e \approx 20°$, after every volume scan, while the transmitter is shut off. Because the estimate $\overline{N}$ is an average of noise power over many more than M samples, the statistical errors should be minimal. On the other hand, $\overline{N}$ is subject to other errors. Figure 2b shows the variation of the National Severe Storms Laboratory (NSSL) Research and Development (R&D) WSR-88D noise power in uncalibrated units (a noise level of 9×10^{-6} units corresponds roughly to a noise power of 5×10^{-12} mW, the specified system noise level) as a function of θ_e when the beam is scanned, while the transmitter was off, across a thunderstorm having the reflectivity field in the vertical cross section shown in Fig. 2a. When $\theta_e = 0.5°$ (the lowest θ_e used operationally), the noise power increases by more than 2 dB. The spikes in $\overline{N}$ are due to exceptionally strong electrical emissions, some of which are more than 8 dB above the background reference level (i.e., the heavy solid curve).

Comparison of data in Fig. 2b with noise power data obtained in scans of clear skies (Fig. 2c) demonstrates that the increase of noise power at $\theta_e < 5°$ is principally due to thermal noise and electrical activity in the storm; increases due to the main beam intersecting the earth begins at about 1° (Fig. 2c); at $\theta_e = 0.5°$, the warm earth accounts for about a 0.4-dB increase of noise power, but some of this increase is due to the sidelobes intersecting the warm earth as evidence by the slow increase of N as θ_e decreases from 10°. Thus, the noise power $\overline{N}$ estimated during the calibration can differ significantly from N if the beam intersects electrically active storms during the 0.075 s when $\overline{N}$ is measured. The WSR-88D compensates, at θ_e increments of 0.5°, for the changes of noise power by monotonically increasing the measured $\overline{N}$ starting at $\theta_e = 5°$ with a 0-dB correction but typically (these corrections can differ from radar to radar) reaching about a +1.7 dB correction at $\theta_e = 0.5°$. As can be seen from Fig. 2b, this does not account for all the increases of $\overline{N}$ that can be associated with thunderstorms. The largest errors in estimates of $\overline{N}$ could occur if the calibration is performed when the beam intersects thunderstorms and radiation from lightning contaminates the noise power estimates. In this case noise power would be overestimated (i.e., $\overline{N} > N$). To mitigate errors in $\overline{N}$ the WSR-88D averages 67% of the $\overline{N}$ from the previous calibration with 33% of the presently measured $\overline{N}$.

Data in Fig. 2b were generated by averaging 128 samples in each of 400 range bins. Because the PRT was 987.2 μs, each data point in Fig. 2b is the average of $M = 5 \times 10^4$ samples collected in about ¼ s (the entire scan took 90 s giving a data spacing of about 0.1° in elevation). The smooth heavy lines in Figs. 2b and 2c are running means (i.e., background reference levels) obtained using a Savitsky–Golay filter (Orfanidis 1996), and the standard deviations about the means has been calculated after clipping the spikes in Fig. 2b. The calculated standard error of the fluctuations in Fig. 2b is more than an order of magnitude larger than that calculated from theory (i.e., $N/\sqrt{M}$), assuming noise samples are uncorrelated. Thus, we suggest that $\overline{N}$ (Fig. 2b) and its fluctuation are principally due to random radiation from electrical discharges and not to statistical fluctuations of uncorrelated thermal noise samples. On the other hand, data in Fig. 2c were collected with $M = 64$ samples per bin times 51 bins = 3.26×10^3 samples; thus a theoretical standard deviation of 1.6×10^{-7} units is calculated, whereas the standard deviation about the running mean computes to 1.7×10^{-7} units, which is in relatively good agreement. In this case N is only due to thermal emissions and the fluctuations are due to the statistical properties of white noise.

c. Spectrum width biases

Melnikov and Doviak (2002) show that the spectrum width bias, σ_v(bias), due to incorrect estimates of N is given by

$$\sigma_v(\text{bias}) = -\sigma_v + \left(\sigma_v^2 - 2\frac{v_a^2}{\pi^2}\frac{N}{S}\frac{\delta N}{N}\right)^{1/2}, \quad (3)$$

where $\delta N = \overline{N} - N$ is the error in noise power estimates, and σ_v is the true spectrum width. Bias is a function of σ_v, and there is a very different bias dependence if noise power is overestimated ($\delta N > 0$) versus what it would be if noise power is underestimated ($\delta N < 0$). The bias

is negative (i.e., σ_v is underestimated) if the noise power is overestimated and positive if noise power is underestimated.

Using Eq. (3), the spectrum width bias σ_v (bias) is plotted in Fig. 3 as a function of noise power measurement errors expressed in decibel units (i.e., $10 \times \log_{10}[1 + \delta N/N]$), with the true spectrum width σ_v as a parameter for two values of signal-to noise ratio (SNR) = $10 \log_{10}$ (S/N). In Fig. 3a, SNR = 3.5 dB is the threshold used by the WSR-88D radar, it is seen that if noise power has an error of about +1 dB, σ_v (bias) as large as −2.5 m s^{-1} would occur if $\sigma_v = 2.5$ m s^{-1}. Spectrum widths become imaginary and are set to be equal to zero if $\delta N > (\sigma_v^2 \pi^2 / 2 v_a^2) S$.

To mitigate errors in the analysis of σ_v data, we have used the much larger SNR threshold of 20 dB. As can be seen in Fig. 3b, the bias errors will be constrained to be less than 0.5 m s^{-1}; this value also equals the quantization interval that σ_v estimates are recorded (NOAA 1991). Such large SNR thresholds are rarely used to censor data. Because the default threshold on SNR in the WSR-88D network of weather radars is typically set at about 3.5 dB, significant biases (Fig. 3a) can occur if noise power measurements do not have errors less than 0.1 dB.

d. Variance of σ_v due to low SNR

In addition to biases, the variances of σ_v estimates become unacceptably large when a too-low SNR threshold is used. For example, in order to display large areas of Doppler velocity in weak reflectivity regions, the WSR-88D radars employ (since 1996) an SNR threshold $T_{sD} = 3.5$ dB, instead of the design threshold of 10 dB. Although this threshold is lower than required to meet the design specifications for velocity errors (i.e., ≤1.0 m s^{-1}), the increase in the velocity estimate error is modest. For example, if $\sigma_v = 5$ m s^{-1}, and $v_a = 25$ m s^{-1}, the standard error of $\hat{v}$ is about 1.1 m s^{-1}. Because WSR-88D cannot separately set SNR thresholds for velocity and spectrum width, the same 3.5-dB threshold is used for σ_v estimates, and a standard error of 1.4 m s^{-1} for the spectrum widths is generated (i.e., the variance of the estimate is doubled). Planned upgrades to the WSR-88D's Radar Data Acquisition system will allow separate thresholds to be set for velocity and spectrum width calculations.

If σ_v is small, imaginary width occurrences can be caused by statistical fluctuations in the estimates of signal power, even if SNR = ∞. If the argument of the logarithmic function in Eq. (1) is less than 1, the signal processor in the WSR-88D sets $\hat{\sigma}_v$ to zero. The purpose of the sgn function in Eq. (1) is to identify these imaginary width values and to assign a zero value to them. If N is overestimated ($\overline{N} > N$), and σ_v is small, spectrum width estimates will be negatively biased and excessive occurrence of zero or imaginary width assignments will be made (Melnikov and Doviak 2002). To mitigate errors due to low SNR if $\overline{N} \neq N$, a relatively large SNR threshold (i.e., 20 dB) is employed when analyzing σ_v data (reflectivity displays in this paper use the WSR-88D default SNR). Even then, as can be seen from Fig. 3b, σ_v of weather signals having sufficiently narrow spectra might erroneously be assigned zero values if noise power measurement errors exceed 1 dB.

e. Errors due to improper AGC settings

Incorrect setting of the automatic gain control (AGC) circuit is another source of error in σ_v estimates. If the AGC is properly set, signal levels should not be so strong that they exceed the maximum input level accepted by the analog-to-digital converter (ADC). If signals exceed this level, they are clipped and harmonics of the spectrum are generated (Doviak and Zrnić 1993, their section 7.7.1), increasing σ_v estimates.

Examination of σ_v data at some radar sites showed that unusually significant correlation of large σ_v with regions of high reflectivity is due to improper setting of the AGC (Sirmans et al. 1997). Figure 4 shows the displays of reflectivity (Fig. 4a), and spectrum widths (Figs. 4b,c) obtained on 31 May 1998 from the Sioux Falls, South Dakota (KFSD), WSR-88D radar having an AGC that was improperly set. The field presented in Fig. 4b was censored using a 20-dB overlaid threshold and a 3.5-dB SNR threshold (routinely used by the WSR-88D). Figure 4c is same except that SNR threshold = 20 dB.

The areas of high reflectivity values exceeding 40 dBZ to the east of the radar (Fig. 4a) at about 70-km range are positively correlated with σ_v values exceeding 7 m s^{-1} (Fig. 4c). Assuming the spectral broadening mechanisms are the same, the equally high reflectivity area a bit north of east at about twice the range has noticeably smaller spectrum widths, suggesting that the correlation is with power not reflectivity; this is expected if the AGC is not properly set. The decrease of power by 6 dB, due the doubling of range to that reflectivity area, is sufficient to diminish the amplitude of weather signal so that they are not as severely clipped by the AGC circuit, resulting in a decrease of width values. On the other hand, the high reflectivity region to the east of northeast at a range of about 200 km has associated with it high σ_v. Because the echo powers from this region are an order of magnitude less than those from the region of equal reflectivity at 140 km, it is less likely these are caused by an improperly set AGC.

Also notice (Fig. 4b) the area of large spectrum widths with considerable spatial variability to the west and southwest from 90–230-km ranges. This is an area of weak reflectivity and thus σ_v estimates likely have excessive spatial variance due to low SNR. Furthermore, these estimates could be biased by incorrect measurements of $\overline{N}$. Note that the spectrum widths appear to be biased high because areas closer to the radar have lower

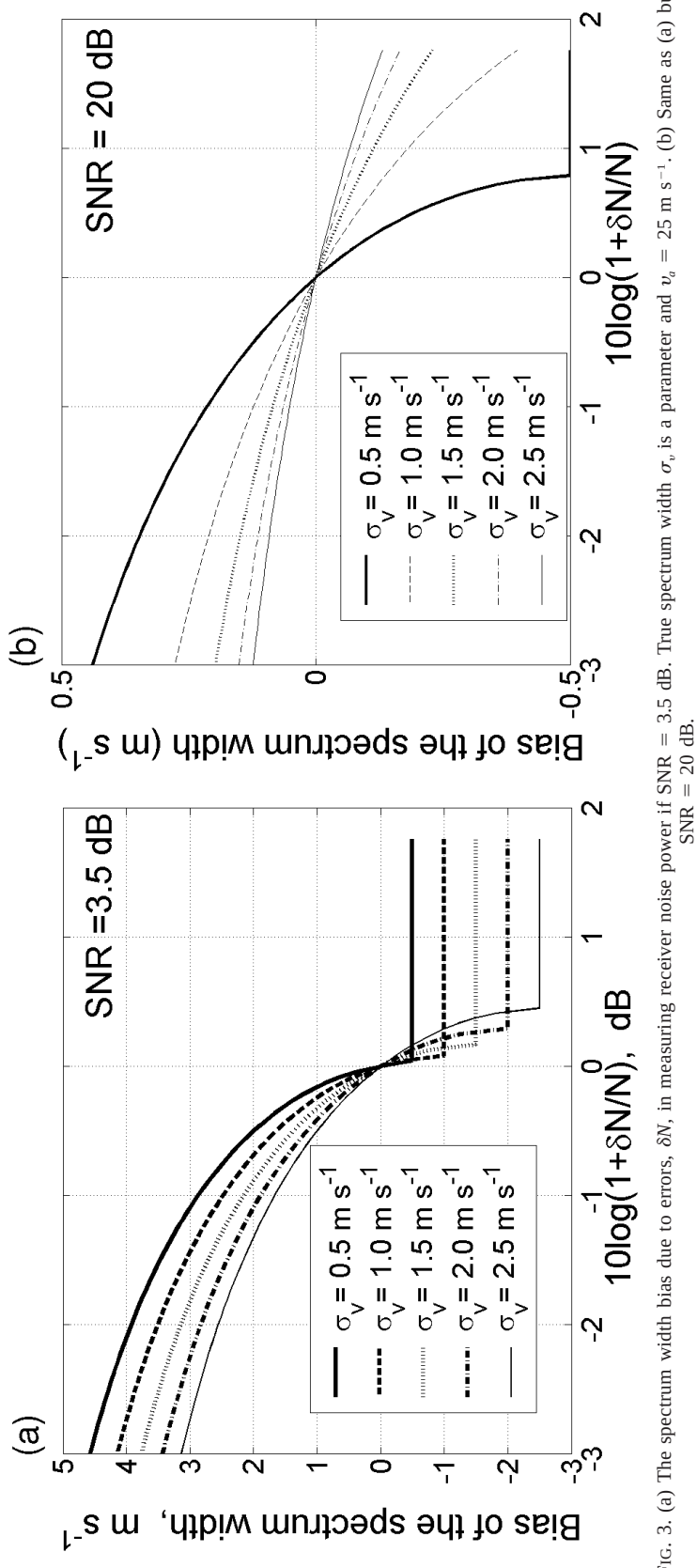

FIG. 3. (a) The spectrum width bias due to errors, δN, in measuring receiver noise power if SNR = 3.5 dB. True spectrum width σ_v is a parameter and $v_a = 25$ m s^{-1}. (b) Same as (a) but SNR = 20 dB.

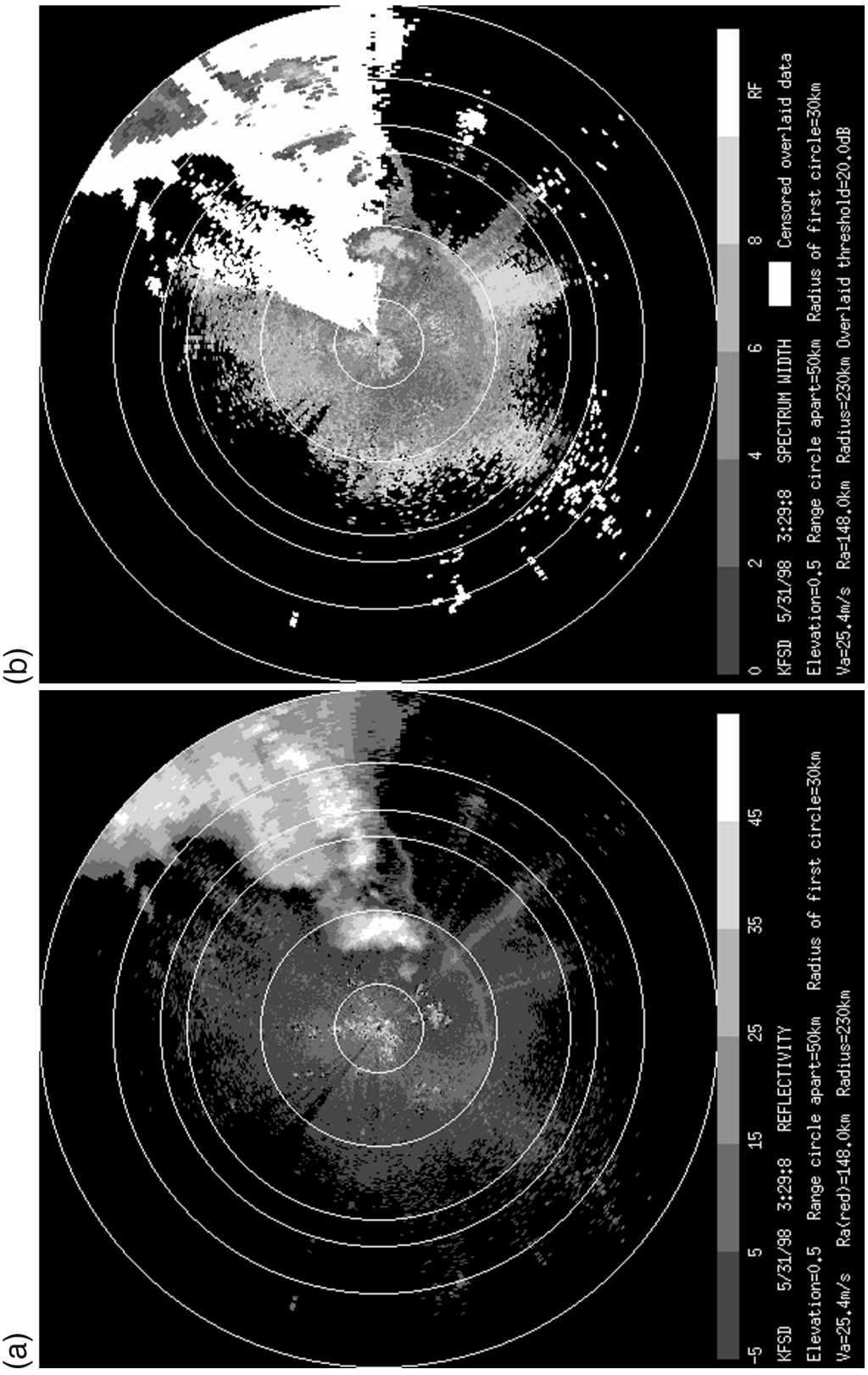

FIG. 4. (a) The reflectivity factor field showing strong reflectivity to the east of the radar site, which produced weather signals that were clipped by improperly set AGC circuits producing biases in spectrum width estimates. (b) The spectrum width field associated with (a); the SNR threshold is 3.5 dB. (c) Same as (b) but SNR = 20 dB.

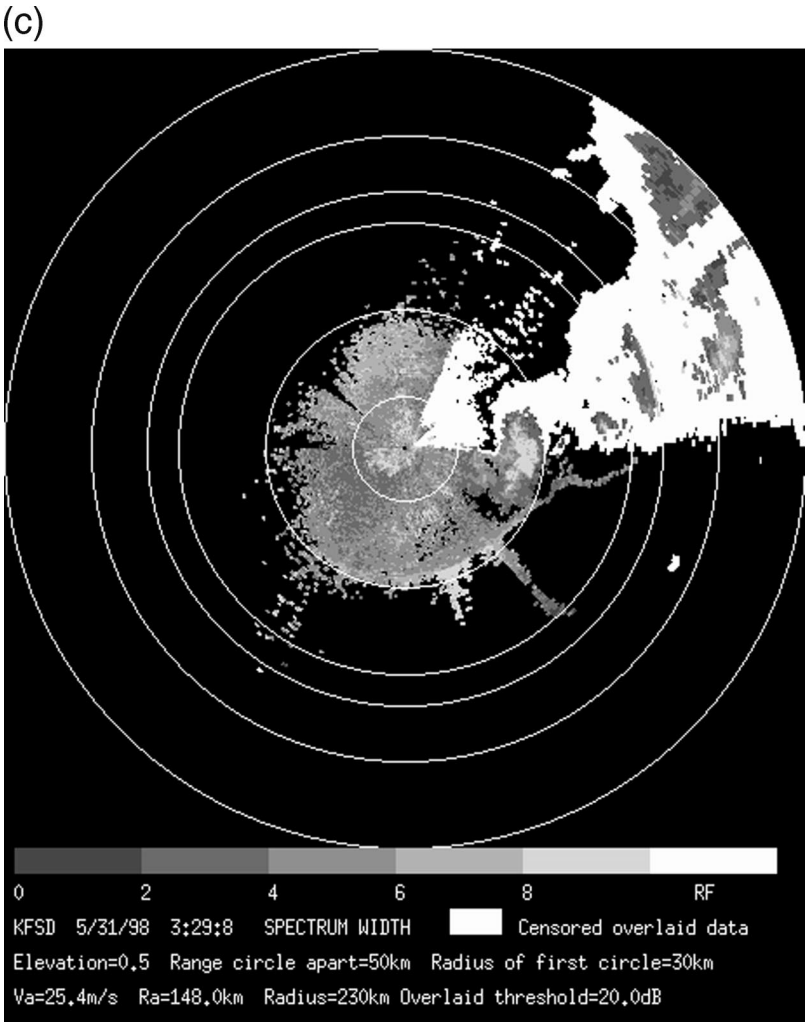

FIG. 4. (*Continued*)

spectrum width values, whereas the meteorological conditions, based on radar observations, appear not to be any different; this positive bias implies that the noise power is underestimated (i.e., biased low). In Fig. 4c, the SNR threshold T_{sD} has been increased to 20 dB, and it is seen that these areas of large spectrum width with considerable spatial variance and suspected bias have been, for the most part, censored.

The area of σ_v larger than 7 m s^{-1} to the southeast at ranges beyond 75 km is due to ground clutter made visible through anomalous propagation conditions, as well as too low an SNR. The mix of clutter and weather signals increases measured σ_v. The anomalous propagation condition is due to the cold air outflow from thunderstorms producing a strong ground-based temperature inversion that bends the lower portions of the beam toward the earth (Doviak and Zrnić 1993); the leading edge of this outflow is marked by the arc of enhanced reflectivity factors seen in Fig. 4a at a range of about 75 km southeast of radar. Thus, σ_v values in this region are not representative of velocity variance within the radar's resolution volumes, and they must be edited by other means that, except for the deductive reasoning just described, are beyond the scope of this work.

3. Censoring potentially erroneous spectrum width data

In order to have reliable σ_v estimates for classification, width data from the WSR-88D archive cannot be used as is without editing. By far the most persistent anomalies appear to be those due to overlaid signals and noise power. Thus an overlaid signal algorithm has been developed to objectively select data that have an in-trip signal power level at least 20 dB higher than the sum of powers from competing out-of-trip signals. That is, an overlaid threshold T_o different from that employed to collect the data is applied to the σ_v field. This is possible because the thresholds employed to collect the

data are lower. Although reflectivity is recorded but power is not, relative powers from the various trips can easily be computed. Thus, the relative signal powers are calculated (absolute signal power is not needed) as a function of range, and the calculations of power ratios for weather signal from the various trips are made.

We also use a relatively large SNR threshold (i.e., $\geq$20 dB) so that improper estimates of noise are less likely to bias our estimates of small σ_v. To compute the SNR from the recorded reflectivity field requires the radar constant and adjustments for atmospheric attenuation. To simplify the calculation, we assume that all WSR-88D radars have the same performance based upon the WSR-88D specifications (Doviak and Zrnić 1993, their Table 3.1). Furthermore, the practical difference between radars is typically only a few decibels, and not enough to affect our analysis and conclusions. In short, a reflectivity factor of 0 dBZ at a range of 230 km is assumed to produce a signal equal to noise power. Thus the SNR (dB) is calculated from the recorded reflectivity factor Z in dBZ, using the formula

$$\text{SNR (dB)} = 20 \log_{10}\left[\frac{230}{r\ (\text{km})}\right] + Z\ (\text{dB}Z).$$

Spectrum widths having zero values sometimes appear to be anomalously large in number. Because $\sigma_v = 0$ could be due to low SNR and incorrect estimates of N, we have not included zero width values in the statistics that are presented in section 4.

Editing data for improper setup of AGC was less quantitative; if positive correlation is detected between large Z (reflectivity factor) and large σ_v in one region, but not in another at about same range, it is assumed that the AGC is correctly set. But if there appears to be a positive correlation in all regions at about the same range, then the WSR-88D data from this radar for this date were not analyzed. Admittedly, it would be better to have an objective method to detect improper AGC settings, and regressing width data with signal power could be useful in detecting strongly clipped signals, especially if the determination of clipping could be automated. Further work should investigate the utility of such regressions. The best method would be to examine the digital values of the in-phase (I) and/or quadrature phase (Q) components at output of the ADC; these values should have a Gaussian distribution with a peak at zero, with very few occurrences at the maximum value. However, digital values of I, Q are not available in the archive II fields.

These editing procedures guarantee that the classified data are more accurate and reliable than if the less stringent thresholds of the WSR-88D were used. Because we have large amounts of data from many radars, and collected for several years, there should be sufficient data to provide meaningful statistics on the relation between spectrum width values and weather classes.

4. Weather classification

We classify the weather into categories that are principally based upon radar observations. The various weather types are subjectively identified, and the region encompassing the selected class is enclosed by a hand-drawn contour within which the data at all elevation angles are processed to gather the statistics of spectrum width. This subjective selection is necessary because any data field could contain more than one class of weather (e.g., strongly convective rain along a squall line and stratiform rain behind it). Fang and Doviak (2001) give examples of the reflectivity fields for each of the examined weather classes.

a. Fair weather

Fair weather echoes are principally associated with two classes of scatterers: 1) refractive index perturbations and 2) biological scatterers such as insects and birds. Radar measurements of the structure parameter C_n^2 of refractive index, airborne in situ measurements of C_n^2 (Doviak and Berger 1980), and numerical models of boundary layers (Burk 1978) suggest that C_n^2 is rarely larger than about 3×10^{-12} m$^{-2/3}$ (Doviak and Zrnić 1993). Using the relationship between Z and C_n^2 [Doviak and Zrnić 1993, their Eqs. (11.104) and (4.33)] this upper limit for C_n^2 corresponds to Z less than 0 dBZ for the WSR-88D. When insects and/or birds are present in sufficient density so that reflectivity fields are spatially uniform, Z can be as much as three orders of magnitude larger than 0 dBZ.

Fair weather is declared if the reflectivity factor field is uniform, confined to 1 or 2 km above ground, and has practically all values less than 10 dBZ. Because our classification is only based on the Z field, the fair weather cases might have significant cloud cover as well as biological scatterers. We have used the 10-dBZ limit in an attempt to eliminate situations where light stratiform rain could satisfy the stipulated conditions for declaring fair weather. For example, using the representative and useful, although not always correct, relation [Doviak and Zrnić 1993, their Eq. (8.22a)]

$$Z_w(\text{dB}Z) = 23 + 16 \log_{10}[R(\text{mm h}^{-1})],$$

between stratiform rain rate R and the reflectivity factor Z_w of water spheres, a 10-dBZ level of reflectivity factor roughly corresponds to a rainfall rate less than 0.15 mm h^{-1}. This is indeed a very light rain and, if present, would not likely be associated with spectrum width values very different from that seen in fair weather. The 10-dBZ limit may not eliminate those cases of ''fair weather'' in which birds and/or insects are present, but, if present, birds and insects can cause spectrum width to be much larger than those values associated with refractive index perturbations (i.e., birds and insects darting about during feeding times can have differential velocities much larger than that associated with shear and turbulence).

b. Stratiform rain

Stratiform rain is assumed if the Z field is fairly uniform over a large area, and has values less than 40 dBZ, which corresponds to a rainfall rate of 11.5 mm h^{-1}. Stratiform rain could be associated with warm fronts in which warm moist air overrides a pool of heavier cold air, or it could be associated with the stratiform rain area behind squall lines, or that evolving from convective precipitation systems.

c. Widespread weak showers

These are, for the most part, numerous isolated convective cells having peak reflectivity less than 45 dBZ, but at least some of the cells have a peak reflectivity values more than 35 dBZ. Each cell typically has diameters less than about 10 km.

d. Isolated severe storms

These are convective cells far from other severe storms that could significantly disturb the environmental flow into the isolated storm. Storms are considered severe if they have large areas in which the peak reflectivity factor is higher than 45 dBZ. These cells usually contain damaging wind, hail, and tornadoes.

e. Severe storm cluster

This is a cluster of cells that are closely spaced (less than about 20 km) and have $Z > 45$ dBZ.

f. Squall line

Precipitation associated with squall lines appear in bands of convection, sometimes attached to a trailing stratiform rain region. But we only examine the statistics of σ_v in regions where $Z > 20$ dBZ. That is, we do not include data from the trailing stratiform region. Following the classification given by Bluestein (1993), this type of weather is further divided into three subclasses. They are embedded areal squall lines, early broken squall lines, and mature broken squall lines. The cells along early broken squall lines are distinctly separate, while the cells merge together along mature broken squall lines.

g. Snow

These data come from winter conditions for which snow is reported by weather stations over large areas, and where Z is at least as large as 10 dBZ. Using the accepted Srivastava–Sekon relation that relates the equivalent rainfall rate R_s of snow to radar measured equivalent reflectivity factor Z_e, but adjusted for the increase of ice particle volume due to the expansion of ice (Doviak and Zrnić 1993, their section 8.4.1.3),

$$Z_e(\text{dB}Z) = 26 + 22.1 \log_{10}[R_s\ (\text{mm h}^{-1})],$$

where R_s is the equivalent water amount in millimeters per hour of the snow fall. A simple conversion of equivalent rainfall rate to the depth of snow per hour is obtained by multiplying R_s with 10. Thus a 10-dBZ equivalent reflectivity factor is produced by a snowfall rate that has a corresponding rainfall rate $R_s = 0.19$ mm h^{-1}; the estimate snow depth rate is about 2 mm h^{-1}, a very light snowfall. So for the most part, the lower limit of 10 dBZ should provide us with σ_v statistics in most regions of significant snowfall. We could have used a smaller lower limit, but judging from the studied reflectivity fields, the number of data not included is relatively small.

5. Results

a. Statistics of various weather classes

The volumetric median values of spectrum width, for the various weather classes described in the previous section and for the storms analyzed to date, are tabulated in Table 1. Each entry is derived from all data within one scan of the entire volume of the weather phenomena being analyzed, and the data number from tens of thousands to more than hundreds of thousands. Also listed are percentages of spectrum widths that exceed 8 m s^{-1} and those that equal zero. When the median value and percentage σ_v larger than 8 m s^{-1} are calculated, zero widths are excluded. Zeros are excluded because their number often appears to be anomalously large, likely due to overestimates of noise power $\overline{N}$. However, the total sample includes zero widths when its percentage is calculated. The Fujita scale ''F'' rating, indicating the severity of the tornado in tornadic storms, is listed in this table. Although the data are limited to one case in some categories, we can make some revealing observations.

Figure 5 shows an example for a case of squall line from the WSR-88D in Tampa, Florida, on 9 March 1998. Figure 5a presents the spectrum width field and shows the subjectively drawn white contour around the data field being analyzed. Figure 5b shows the distribution and cumulative probability of the spectrum widths enclosed by the white contour in Fig. 5a. Because the data are collected in radar or polar coordinates, weather elements close to the radar would have many more points than like elements that are at more distant ranges; thus there would be an unequal weighting of the σ_v data. Therefore, we have interpolated data to a Cartesian coordinate system with grid spacing of 250 m, about the best resolution of the radar, so that there are equal numbers of grid points per unit area, independent of range. The upper curve in Fig. 5b displays the probability distribution (in percent) of σ_v for all elevation angles that have data within the vertical column enclosed by the hand-drawn contour, and which have been censored using a 20-dB overlaid threshold and a 20-dB signal-to-

TABLE 1. Median values of spectrum width (m s^{-1}) in a single volume scan, and the percentages larger than 8 m s^{-1} and of those equal to zero.

Fair weather	($-5 \le Z \le 10$ dBZ)		
(i) 13 May 1998 Oklahoma City, OK	1.9; 0.8%; 5.5% ($0 \le Z \le 20$ dBZ)	Fair weather without birds	
(ii) 1 Aug 2000 Oklahoma City, OK	3.0; 1.8%; 3.8%	Bird-related echoes	
Stratiform rain	($20 \le Z \le 40$ dBZ)		
(i) 27 May 1995 Des Moines, IA	1.5; 0.2%; 19.1%		
(ii) 24 Jan 1997 Nashville, TN	1.7; 1.1%; 14.3%		
(iii) 30 Oct 1999 Oklahoma City, OK	2.3; 1.6%; 8.6%		
Snow	($10 \le Z \le 30$ dBZ)		
(i) 26 Jan 2000 Oklahoma City, OK	2.0; 0.0%; 6.8%		
(ii) 16 Jan 1994 Saint Louis, MO	1.7; 1.0%; 18.0%		
(iii) 6 Jan 1995 Saint Louis, MO	1.9; 0.4%; 12.0%		
Widespread showers	($20 \le Z \le 45$ dBZ)		
(i) 9 Mar 1998 Tampa, FL	2.1; 0.0%; 7.8%		
Severe storm cluster	($20 \le Z \le 70$ dBZ)	($20 \le Z < 40$ dBZ)	($40 \le Z \le 70$ dBZ)
(i) 3 May 1999 Oklahoma City, OK	2.9; 3.0%; 5.3%	2.8; 2.3%; 5.9%	3.9; 7.1%; 1.3%
Squall lines	($20 \le Z \le 70$ dBZ)		
(i) 15 Apr 1994 Saint Louis, MO	4.0; 7.2%; 0.5%	Embedded areal	
(ii) 9 Mar 1998 Tampa, FL	5.4; 14.7%; 0.1%	Embedded areal	
(iii) 31 May 1998 Albany, NY	2.1; 0.1%; 13.9%	In earlier stage of broken line	
(iv) 31 May 1998 Albany, NY	3.0; 1.3%; 4.4%	Embedded and broken	
(v) 23 Jan 1996 Shreveport, LA	2.5; 0.9%; 7.9%	In mature stage of broken line	
Isolated severe storms	($20 \le Z \le 70$ dBZ)	($20 \le Z < 40$ dBZ)	($40 \le Z \le 70$ dBZ)
(i) 3 May 1999 (F5) Oklahoma City, OK	1.8; 0.6%; 20.1%	1.8; 0.7%; 21.2%	1.8; 0.6%; 18.3%
(ii) 31 May 1996 (F3) Aberdeen, SD	1.4; 0.4%; 22.2%	1.4; 0.4%; 21.9%	1.4; 0.3%; 23.0%
(iii) 16 Apr 1998 (F3) Nashville, TN	1.7; 0.7%; 27.8%	1.7; 0.8%; 26.8%	1.7; 0.5%; 29.5%

noise ratio (SNR), and meet the specified restrictions (i.e., 20 dB$Z \le Z \le$ 70 dBZ). Although reflectivity factors reach values as large as 70 dBZ, examination of the data suggested that the AGC was properly set.

The σ_v data are provided with 0.5 m s^{-1} resolution, and these data are therefore accumulated into 0.5 m s^{-1} intervals for presentation in Fig. 5b. The lower plot is the cumulative distribution, also for the entire volume. We derive the median value of spectrum width from the cumulative distribution. Also indicated on this figure are the total number of grid points and the percent of data for which the spectrum width exceeds 8 m s^{-1}.

An 8 m s^{-1} value is chosen because simulations of the performance of SZ phase code algorithms to separate overlaid signals (to estimate Doppler velocities associated with the weaker signal) suggest that separation is unlikely for spectra with widths larger than 8 m s^{-1} (Sachidananda et al. 1998). This limit is dependent, however, on the ratio of overlaid signal powers and the σ_v of both spectra. For example if σ_v of the weaker signal is about 4 m s^{-1}, and the signal has power 10 dB below the stronger signal, signal separation is possible if the stronger signal σ_v is less than about 7 m s^{-1} (Sachidananda et al. 1998, their Fig. 5.6). Figure 5c presents the spectrum width field associated with Fig. 5a, but at an elevation angle of 3.3°. Note the ring of enhanced σ_v values at the relatively constant range of 100 km. This feature suggests a layer of shear at an altitude of about 6.3 km, and is likely the same shear layer responsible for the large σ_v seen at long ranges in Fig. 5a. The σ_v values along the squall line rainband continue to be large, but take on the appearance of separated convective elements.

b. Discussion

Fair weather cases fall into two subcategories: bird-related echoes (1 August 1998 in Table 1) and fair weather without birds (13 May 2000 in Table 1). In fact we cannot definitely eliminate the existence of birds. When we say ''without birds'' we mean that there is no evidence supporting the existence of bird-related echoes, and the birds' contribution to the σ_v field is small compared to the contribution from C_n^2 or/and insects. The median σ_v value for fair weather without birds is 1.9 m s^{-1}.

Zhang et al. (2002) proposed an algorithm that allows one to separate the bird-related echoes from meteorological ones. To simplify the problem, a believed bird-related case is subjectively picked out in this study. This case started with a spot in the Z, then expanded and formed a ring pattern whose radius became larger with time. This pattern is same as that observed by Sporer et al. (2000), who verified, through bird observations with a team of people, that the Z pattern was formed by birds. Comparing the statistics in Table 1, one sees that the median σ_v value of associated with suspected bird echoes is 3 m s^{-1}, considerably larger than that in

the fair weather case without birds (or else the birds in that case have less velocity dispersion).

All three isolated severe storms listed in Table 1 were producing tornados at the time of the analysis. Thus, their very low median σ_vs are surprising, particularly for 3 May 1999 storm that devastated Moore, Oklahoma, with an F5 tornado. Nevertheless, σ_v in the region close to the tornado was larger than 8 m s^{-1} (this region occupied a small portion of the total storm volume and does not affect the calculation of the medians). Median σ_v values inside the high-reflectivity core are about same as those outside the core, for all three cases.

Because zero values have been excluded from the media value statistics, the median value in these tornadic storms would even be smaller if they were included. However, the large percentage (i.e., 20% to ≈30%) of zero values in these storms is surprising. Undoubtedly, some of these zeros could be due to statistical fluctuations that cause the estimated argument of the logarithmic function in Eq. (1) to be less than one, and thus a true small σ_v could be assigned to a zero category. On the other hand, assuming that the errors of estimation due to statistical fluctuation are normally distributed about their expected values and noting that we use an SNR threshold of 20 dB, the standard error of uncensored σ_v estimates is about 1 m s^{-1} or less (Doviak and Zrnić 1993; their Fig. 6.6 for $v_a \approx 21$ m s^{-1}, and $M \approx 50$). Thus, we calculate that statistical fluctuations in the estimation cannot contribute more than about 7% of the number of observed zeros and other mechanisms must cause the large percent of zero widths. One possibility is that noise power $\overline{N}$ is overestimated which, as can be seen in Fig. 3b, causes spectrum widths to be underestimated; this would increase the number of zero values. For example, if there is a +3 dB error in noise power measurements, the maximum bias computed from Eq. (3) is less than 1 m s^{-1}, which occurs for a true width of about 1 m s^{-1}. Larger spectrum widths have even smaller biases as can be seen from Fig. 3b. It seems unlikely that such large positive noise power errors could be made in three different radars. On the other hand, if during calibration, the beams passed through electrically active storms, the noise power measurements could all be biased positively (Fig. 2b) and thus all spectrum widths would be biased low. A more detailed study of the calibration procedure and comparisons of noise power measurements in thunderstorm environments are required to establish whether the low σ_v is due to errors in noise power measurements during calibrations, or σ_v is indeed very small in isolated storms. This study is beyond the scope of this paper. It should be noted, however, that the data for the severe storm cluster (Table 1) were obtained with the same radar at the same time, but the percent of zero values is much less for the storm cluster. This suggests that many of the zero values are not due to excessive errors in noise power measurements, and thus it appears that widths in the isolated tornadic storms are unusually small.

Because the measured σ_v comes from contributions of both shear and turbulence, the spectrum width associated with turbulence in the tornadic storms should be even smaller than that tabulated in Table 1, suggesting unexpectedly weak turbulence in these violent storms. The low median values in these tornadic storms are in contrast to those in squall lines, severe storm clusters, and even widespread showers. Furthermore, supercell storms often form in an environment with large shear that contributes to increased spectrum width. Perhaps the relatively isolated locations of the storms allowed them to have a well-organized structure that permits them to last a long time and have a relatively laminar flow. This view is consistent with the interpretation that these tornadic storms are steady-state supercell thunderstorms.

Supercells interact with the environment in such a way as to organize a steady flow of ascending and descending air within the storm while they propagate either to the left or right of the mean tropospheric wind with a velocity that allows them a steady interaction with the large-scale environment (Browning 1982). Perhaps the supercells, forming in a relatively undisturbed environment, have well-separated up- and downdrafts that interact less and thus have less turbulence. Furthermore, rotating supercell storms are characterized by high positive helicity that suppresses nonlinear energy transfer and turbulence generation (Lilly 1986). So these ''unexpected'' low σ_v could be evidence of high helicity in supercell storms, which is consistent with Wu's (1992, 1990) deduction. Brandes et al. (1988) observed large helicity in updraft regions of two tornadic supercells. They attributed the longevity of storms and less small-scale features in updraft regions to the high positive helicity and the upward-accelerating pressure gradients. It is noteworthy that they also observed weak positive or negative helicity in the downdraft region of the storms. However, our data suggest that the entire storm, encompassed by the 20-dBZ contour, has less turbulence. Further study is needed to understand why the median spectrum values obtained for entire volume of tornadic storm are unexpectedly small.

On the other hand, storms in a cluster, observed on 3 May 1999 at the same time as the isolated severe storm but at longer ranges (i.e., 70–130 versus 0–35 km), have significantly larger median spectrum width values (3.9 versus 1.8 m s^{-1}) in the regions of high Z (i.e., ≥40 dBZ), and more than an order of magnitude larger percent of $\sigma_v > 8$ m s^{-1}. The median value for all regions of $Z > 20$ dBZ decreases from 3.9 to 2.9 m s^{-1} because of the lower spectrum widths (i.e., median value equal to 2.8 m s^{-1}) in regions of lower Z (i.e., between 20 and 40 dBZ) persist over much larger areas. The velocity field (not displayed) in the severe storm cluster region exhibits a large spatial variance that supports the observed large σ_v values. It is noteworthy that

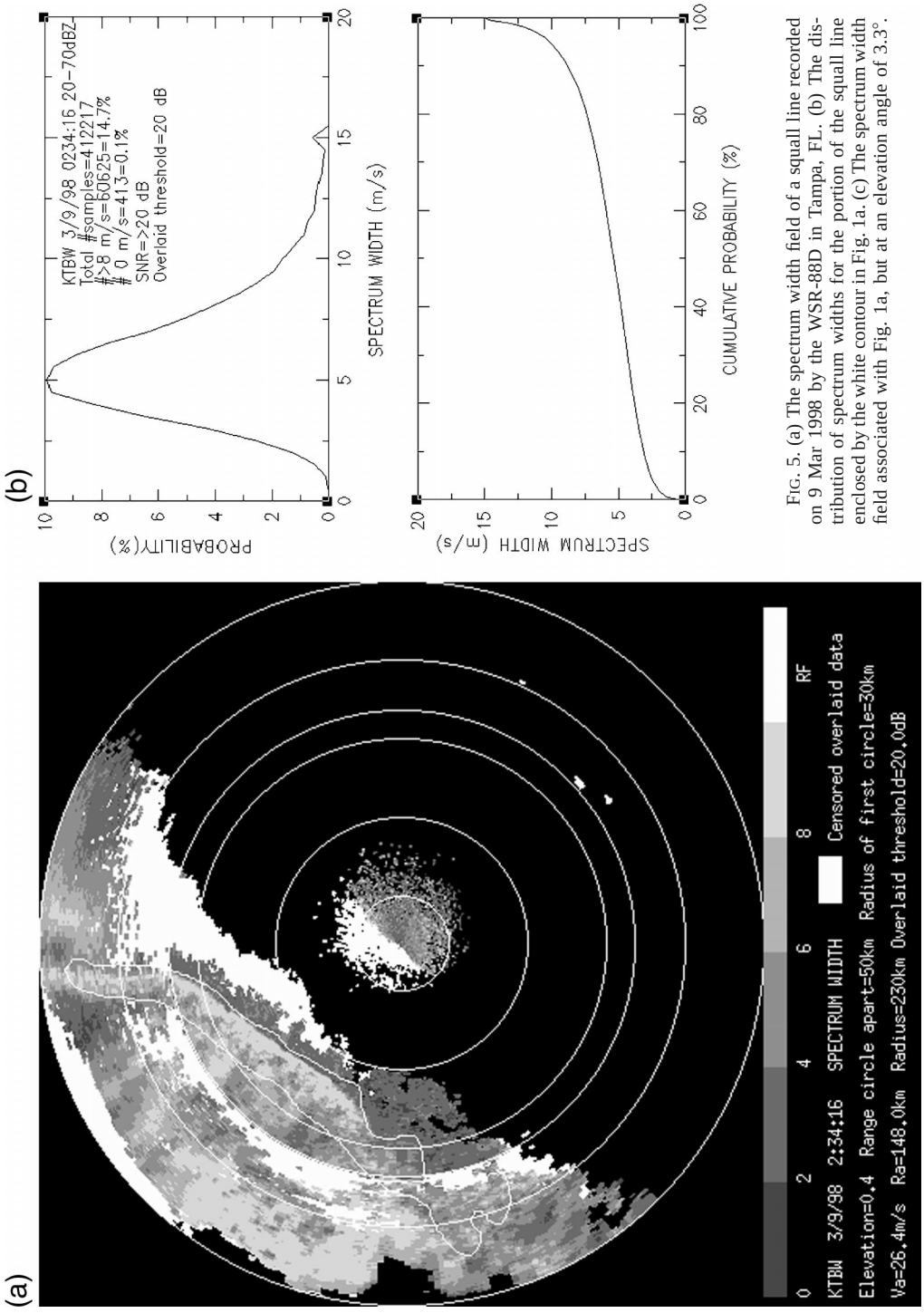

FIG. 5. (a) The spectrum width field of a squall line recorded on 9 Mar 1998 by the WSR-88D in Tampa, FL. (b) The distribution of spectrum widths for the portion of the squall line enclosed by the white contour in Fig. 1a. (c) The spectrum width field associated with Fig. 1a, but at an elevation angle of 3.3°.

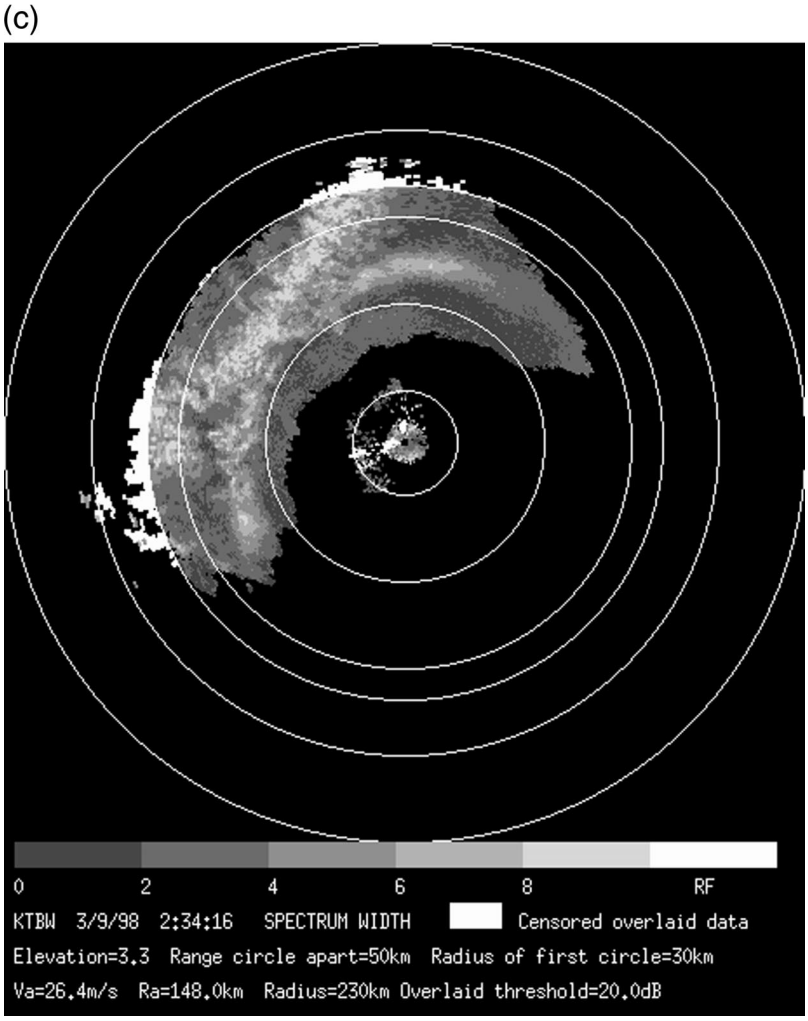

FIG. 5. (*Continued*)

because the beamwidth is larger for the more distant storms, it might be expected that larger variance of Doppler velocities within the beam would be observed, and thus spectrum widths would, on average, be larger. We have examined a case that clearly shows that radar-measured spectrum width decreases when a storm moves toward radar and then increases when a storm moves away. On the other hand, the σ_v in the low Z regions is not as large as that in the higher Z regions (Table 1), suggesting that the high Z cores are more turbulent, contain stronger shear, or both.

To make a meaningful examination of turbulence we need to separate the contributions from shear and turbulence, and also examine the spatial distribution of turbulence throughout the storm. The contribution of the shear to the observed σ_v needs to be determined using, for example, the methods of Istok and Doviak (1986) before we can draw a conclusion concerning the level of the turbulence in any weather category. This has not been done. Nevertheless, it is interesting to note that the median value of σ_v in the weak reflectivity regions (i.e., between 20 and 40 dBZ) of the severe storm cluster is smaller than that in the high-reflectivity regions (i.e., between 40 and 70 dBZ), whereas they are identical in the two regions of the isolated severe storms. Since only one case of severe storm clusters is investigated, it is not clear whether or not this observed difference is also true in other similar cases.

The spectrum width of the widespread shower case equals that for broken-line squall line in its early stage [i.e., squall line (iii) in Table 1]. This preliminary result is consistent with the fact that both of them often form in an environment of weak shear and their cells often behave like ordinary cells.

The largest σ_v cases (i.e., those that have a median $\sigma_v > 4$ m s^{-1}) are associated with the high Z region of embedded areal squall lines; in some cases almost 15% of the σ_v data exceed 8 m s^{-1}. But the σ_v of squall lines spans a wide range of median values from about 2.1 to 5.4 m s^{-1}. Squall lines may form in environments in

which vertical shears of horizontal winds are different, and this might cause differences in the structure of the squall line and the σ_v medians seen among squall lines. Furthermore, the median σ_v value would also be a function of the squall line's stage of development. More detailed investigations are necessary to reveal the physical reasons behind these differences.

6. Summary and conclusions

Spectrum width, σ_v, one of the three data fields available to radar meteorologists using the WSR-88D weather radars, is rarely used operationally. Yet it has the potential to improve our understanding of severe weather (Lemon 1999) and warnings of hazards to safe flight (Cornman et al. 1999). Furthermore, σ_v data are valuable in determining the performance of various signal-processing schemes that are offered as candidates to improve radar performance. We review the reasons why this potentially valuable data field has been ignored, and propose methods of editing spectrum width data field so that confidence can be ensured for its value in studies of weather phenomena, and in applications of engineering solutions to some of the problems that arise when radars are used to observe weather. Some conclusions that can be obtained based on this preliminary study are as follows.

To have reliable spectrum width data for analysis, the spectrum width field observed by WSR-88D should be censored using a 20-dB overlaid threshold, a 20-dB SNR threshold, and rejecting datasets for that day if there is evidence that large σ_v values are correlated with large echo powers. The surprisingly small median σ_v for many studied weather classes suggest that range–velocity ambiguity mitigation techniques proposed for WSR-88D might work better than anticipated. On average, isolated severe storms, fair weather without birds, widespread showers, broken squall lines in early stages, and stratiform rain and snow, have median σ_v less than about 2 m s^{-1}. Largest σ_v with median values exceeding 4 m s^{-1} are found in the convective cores of squall lines embedded in stratiform rain regions. Clusters of severe storms and storms along broken squall lines appear to have median σ_v between these two regimes. More case studies are required to learn whether or not this categorization is general. Further studies are needed to reveal the physics behind unexpected small median σ_v in isolated severe storms, and the wide variations of median σ_v among squall lines.

Acknowledgments. This research was partially supported by the Radar Operation Center (ROC) of the National Weather Service, in Norman, Oklahoma. Dr. Larry Cornman, of the Research Applications Program of National Center for Atmosphere Research, has been instrumental in obtaining support for this effort. Support for this research is in response to requirements and funding by Federal Aviation Administration (FAA). The views expressed are those of authors and do not necessarily present the official policy or position of the FAA. We also acknowledge the continued encouragement and comments from Dr. D. S. Zrnić of the NSSL, and discussions with Mr. Dale Sirmans at ROC, Dr. D. Lilly at the University of Oklahoma, and Dr. P. Zhang of CIMMS.

REFERENCES

Bluestein, H. B., 1993: *Synoptic-Dynamic Meteorology in Midlatitudes.* Vol. 2. Oxford University Press, 520–526.

Bohne, A. R., D. J. Smalley, F. I. Harris, S. L. Tung, and P. R. Desrochers, 1997: New application for Doppler spectrum width in storm analysis. Preprints, *28th Int. Conf. on Radar Meteorology,* Austin, TX, Amer. Meteor. Soc., 380–381.

Brandes, E. A., R. P. Davies-Jones, and B. C. Johnson, 1988: Streamwise vorticity effects on supercell morphology and persistence. *J. Atmos. Sci.,* **45,** 947–963.

Browning, K. A., 1982: General circulation of middle-latitude thunderstorms. *A Social, Scientific, and Technological Documentary,* E. Kessler, Ed., Vol. 2, NOAA, U.S. Dept. of Commerce, U.S. Government Printing Office, 211–247.

Burk, S. D., 1978: Use of a second-moment turbulence closure model for computation of refractive index structure coefficients. Naval Environmental Prediction Research Facility Tech. Rep. TR-78-04, Monterey, CA, 58 pp.

Cornman, L. B., R. K. Goodrich, R. Frehlich, B. Sharman, and N. Beagley, 1999: The detection of convective turbulence from airborne Doppler radar. Preprints, *29th Conf. on Radar Meteorology,* Montreal, QC, Canada, Amer. Meteor. Soc., 864–867.

Doviak, R. J., 1999: Atmospheric turbulence and its detection by radar. *Aviation Weather Surveillance Systems: Advanced Radar and Surface Sensors for Flight Safety and Air Traffic Management,* P. Mahapatra, Ed., IEE and AIAA, 453 pp.

——, and M. J. Berger, 1980: Turbulence and waves in the optically clear planetary boundary layer resolved by dual Doppler radars. *Radio Sci.,* **15,** 297–317.

——, and D. Zrnić, 1993: *Doppler Radar and Weather Observations.* Academic Press, 562 pp.

Fang, M., and R. J. Doviak, 2001: Spectrum width statistics of various weather phenomena. National Severe Storms Laboratory Report, Norman, OK, 62 pp.

Istok, M. J., and R. J. Doviak, 1986: Analysis of the relation between Doppler spectrum width and thunderstorm turbulence. *J. Atmos. Sci.,* **43,** 2199–2214.

Lemon, L. R., 1999: Operational uses of velocity spectrum width data. Preprints, *29th Int. Conf. on Radar Meteorology,* Montreal, QC, Canada, Amer. Meteor. Soc., 776–779.

Lilly, D. K., 1986: The structure and propagation of rotating convective storms. Part II: Helicity and storm stabilization. *J. Atmos. Sci.,* **43,** 126–140.

Melnikov, V. M., and R. J. Doviak, 2002: Spectrum widths from echo power differences reveal meteorological features. *J. Atmos. Oceanic Technol.,* **19,** 1793–1810.

NOAA, 1991: NEXRAD Technical Requirements. Report #R400-SP401A, November, 190 pp. [Available from NEXRAD Joint System Program Office, Silver Spring, MD, 20910.]

Orfanidis, S. J., 1996: *Introduction to Signal Processing.* Prentice Hall, 798 pp.

Sachidananda, M., D. S. Zrnić, R. J. Doviak, and S. Torres, 1998: Signal design and processing techniques for WSR-88D ambiguity resolution, part II. National Severe-Storms Laboratory Report, 105 pp.

Sirmans, D. R., R. Gunther, and J. Windes, 1997: Engineering study

of spectrum width anomaly. Informal Report submitted to the Operational Support Facility of the National Weather Service, Norman, OK, 10 pp.

Sporer, M. B., K. A. Lombardy, and J. Conklin, 2000: Investigation of bird radar echoes detected by the WSR-88D Doppler radar at NWSO Binghamton, NY. *Proc. Symp. on Weather Radar and Its Application to Ornithology,* Houston, TX. [Available online at http://www.afonet.rg/english/abstracts.html.]

Wu, W. S., 1990: Helicity buoyant convection. Ph.D. thesis, University of Oklahoma, 161 pp.

——, D. L. Lilly, and R. M. Kerr, 1992: Helicity and thermal convection with shear. *J. Atmos. Sci.,* **49,** 1800–1809.

Zhang, P. F., Q. Xu, and A. V. Ryzhkov, 2002: Identification of biological scatters and radar data quality control. Preprints, *21st Conf. on Severe Local Storms,* San Antonio, TX, Amer. Meteor. Soc., 208–209.